Dynamic Admittance Parameterization of Non-Prehensile Multi-Robot Transport with Optimal Coordinated Planning

Calvin Stahoviak [1] * **Xavier Barr** [1] * **G. Matthew Fricke** [1, ⋆] *
Sachi Barnaby [1] * **Melanie E. Moses** [1,2,3] *
Jonathon E. Slightam [4] **

* *University of New Mexico, Albuquerque, NM 87131 USA (e-mail: cstahoviak@unm.edu, xbarr@unm.edu, mfricke@unm.edu, sbarnaby505@unm.edu, melaniem@unm.edu)*
** *Sandia National Laboratories, Albuquerque, NM 87185 USA (e-mail: jslight@sandia.gov)*

Abstract: Non-prehensile coordinated mobile manipulation is challenging because interactions between the robot bases and payload must be managed carefully. We present the **Dyn**amic **A**dmittance parameterization of Non-Prehensile **M**ulti-robot Transport with **O**ptimal Coordinated Planning (DYNAMO) architecture for payload transport using dual nonholonomic 4DOF mobile manipulators. DYNAMO minimizes snap and angular momentum change along a payload path and adapts arm motion to interaction forces. In hardware experiments DYNAMO achieves longer and more reliable payload transport than position-based methods, providing a practical foundation for multi-robot cooperative grasp-free manipulation.

Keywords: Robotics, Path Planning and Motion Control, Multi-agent and Networked Systems

1. INTRODUCTION

Among the various multi-robot tasks, cooperative transportation of objects without grasp-points presents particular challenges in dynamics and control. Non-prehensile manipulation is much more challenging than prehensile manipulation (e.g. grasping or caging) in that the payload must be sustained using frictional and pushing forces. While caging end-effectors can handle grasp-point free objects, non-prehensile manipulation via a flat-plate end-effector demonstrates adaptive control law alone is sufficient. Multi-robot cooperative transportation allows for the manipulation of larger objects (scaling with the number of agents) and objects without grasp points via non-prehensile manipulation. Practical applications include robotic warehouse logistics, cleanroom laboratories, and "lights-out" manufacturing facilities.

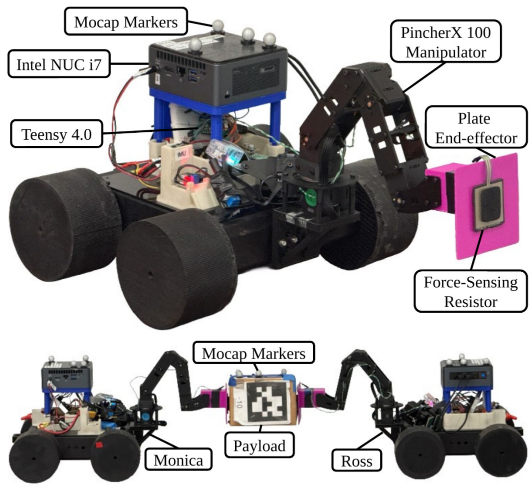

Fig. 1. Joint Integrated Admittance, Navigation, and Transport (JiANT) robots are modified Swarmies made from off-the-shelf and 3D printed components.

To address this challenge, we introduce the **Dyn**amic **A**dmittance parameterization of Non-Prehensile **M**ulti-robot Transport with **O**ptimal Coordinated Planning (DYNAMO) system, in which two robots cooperate to transport a payload without grasp-points. A coordinated optimal planner generates the desired trajectory of transport, and a dynamically parameterized admittance model addresses robot pose uncertainty during transport. In our

⋆ This work was supported by Laboratory Directed Research and Development program at Sandia National Laboratories. Sandia National Laboratories is a multi-mission laboratory managed and operated by National Technology & Engineering Solutions of Sandia, LLC., a wholly owned subsidiary of Honeywell International, Inc., for the U.S. Department of Energy's National Nuclear Security Administration under contract DE-NA000352. This paper describes objective technical results and analysis. Any subjective views or opinions that might be expressed in the paper do not necessarily represent the views of the U.S. Department of Energy or the United States Government.
[1]Department of Computer Science, University of New Mexico. [2]Department of Biology, University of New Mexico, Albuquerque, NM, USA. [3]Santa Fe Institute. [4]Unmanned Systems and Autonomy Research and Development at Sandia National Laboratories, Albuquerque, NM, USA.
*Correspondence: `cstahoviak@unm.edu`; `cjstahoviak@gmail.com`

experiments a payload (see Figure 1) was successfully transported 100% of the time, whereas a position controller achieved 0% success and a static admittance controller achieved only 5–25 % success.

Since our system is demonstrated on physical mobile hardware, it departs from prior work in simulation or fixed-base robot arms (Hichri et al. (2019); Liu and Miah (2024)). Our method is most closely related to caging-based cooperative transport (Tuci et al. (2018)). This foundation of our approach, the natural admittance controller introduced by Newman (1992) models compliant behavior via mass-spring-damper systems. Methods for analytically designing admittance or impedance controllers include passivity methods, which can be leveraged for actively changing parameters to improve stability or controller convergence Slightam et al. (2021); Slightam and Griego (2023). For surveys of non-admittance control strategies, see Amirkhani and Barshooi (2022). Leader–follower approaches are reviewed in Jinyan Shao et al. (2005); An et al. (2023). Yufka and Ozkan (2015) demonstrate a multi-robot system where the object is rigidly affixed to the robots, eliminating the need for compliance. In purely theoretical work, robot–payload teams are modeled as a unified system using Jacobians to optimize coordination (Chen and Kai (2018); Qin et al. (2022)) assuming perfect knowledge of dynamics.

Admittance control has been applied in single-robot systems (McArthur et al. (2024); Gholampour et al. (2025)), multi-arm settings (Li et al. (2019)), and simulations (Barawkar et al. (2017)). Carey and Werfel (2021) simulate linear transport of a grasped payload using impedance control. In contrast, DYNAMO enables transport along curved trajectories with compliant, non-grasping end-effectors in hardware. Duan et al. (2018) demonstrate an adaptive method that tracks dynamic forces on a single manipulator by adjusting impedance parameters online. In contrast, we apply adaptive tuning framework to multi-robot non-prehensile mobile transport to enhance performance under uncertain sensing and actuation.

2. METHODS

We implemented the proposed admittance control strategy for non-prehensile cooperative manipulation, describe the construction of JiANTs, and the experimental design used to evaluate DYNAMO's performance in hardware trials. All numerical values are reported to two significant figures unless otherwise noted. The robots are named Monica and Ross in reference to a TV show in which a group of friends struggle to cooperatively carry a couch.

2.1 Analytical Methods

Static Admittance Control Hogan and Buerger (2004) define an admittance controller by the relationship between force and motion at the "port of interaction". By modeling the compliant mechanical behavior of a mass-spring-damper system, forces at the end-effector are translated into smooth motion trajectories that prevent damaging the manipulator or the payload. The general formula for admittance control in one-dimensional free space is given in Equation (1) where F_{ext} is the external force, M is the mass, B is the damping, K is the stiffness, and x is the relative distance from the virtual position.

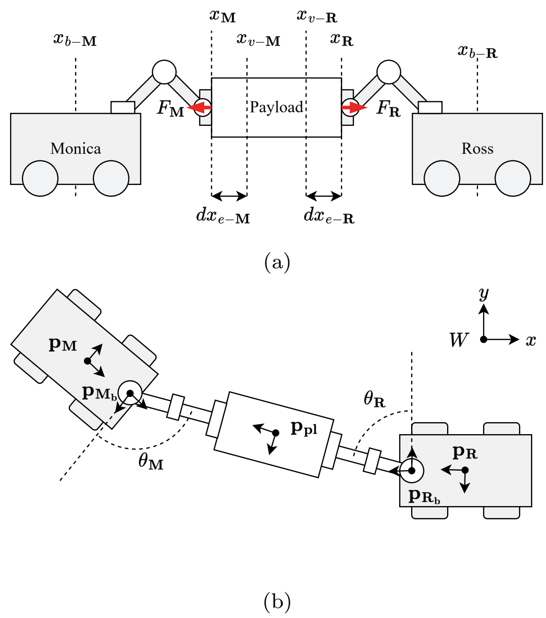

Fig. 2. (a) Lateral view of the transportation setup. (b) View from above of the payload, mobile base, and manipulator base poses labeled. Heading adjustment angles θ_{M} and θ_{R}.

$$F_{\text{ext}} = M\ddot{x} + B\dot{x} + Kx \tag{1}$$

We introduce a frame of reference by defining a virtual set point x_{v} as shown in Equation (2) where x is the relative distance from x_{v}. By setting x_{v} inside of the payload, a controlled force, F_{ext}, can be exerted.

$$F_{\text{ext}} = M\ddot{x} + B\dot{x} + K(x - x_{\text{v}}) \tag{2}$$

With $\dot{x} = 0$ and $\ddot{x} = 0$ and step size $\Delta t = 0.002$ (500 Hz update rate), Euler's method is used to compute the displacement $(x_t - x_{\text{v}})$ generated by the admittance controller in Equation (5).

$$\ddot{x}_t = \frac{1}{M}(F_{\text{ext}} - B\dot{x} - K(x_{t-1} - x_{\text{v}})) \tag{3}$$

$$\dot{x}_t = \dot{x}_{t-1} + \ddot{x}_t \Delta t \tag{4}$$

$$x_t - x_{\text{v}} = (x_{t-1} - x_{\text{v}}) + \dot{x}_t \Delta t \tag{5}$$

This controller is implemented on both JiANT robots, modeling each as a mass-spring-damper system on either side of the payload as seen in Figure 2a. This dual-admittance is necessary in eliminating the potential of high impact forces, which could damage the manipulator or the payload. The parameters for the static admittance controller (Table 1) were initially chosen using the critical damping heuristic, $B_{\text{crit}} = 2\sqrt{MK}$, then hand tuned to maintain consistent contact between each manipulator and the payload prior to driving.

Online Dynamic parameterization of Admittance-Based Control The static admittance controller in Section 2.1.1 is parameterized for a fixed inter-robot distance, which changes during transportation.

We propose a dynamically parameterized admittance controller that updates K and x_{v} during transportation based

Table 1. Admittance controller parameters for static and dynamic parameterization.

Symbol	Meaning	Default Value
x_{v}	Default virtual position	0.25
K	Default stiffness	60
B	Default damping	70
M	Default mass	5
α_x	Gain for x_{v} update	0.5
α_K	Gain for K update	30

on inter-robot distance. These update rules are defined as follows:

$$x'_{\mathrm{v}} = x_{\mathrm{v}} + \alpha_x e \tag{6}$$

$$K' = K + \alpha_K e \tag{7}$$

where $e = \|\mathbf{p}_{\mathrm{M}} - \mathbf{p}_{\mathrm{R}}\|$ is the magnitude of the error in relative position between Monica and Ross, x_{v} is the default parameter for virtual position, K is the default parameter for stiffness, α_x is the scaling factor for virtual pose, and α_K is the scaling factor for stiffness. Modifying Equation (2) to use the adaptive variables x'_{v} and K' arrives at the dynamic admittance controller in Equation (8).

$$\begin{aligned} F_{\mathrm{ext}} &= M\ddot{x} + B\dot{x} + K'(x - x'_{\mathrm{v}}) \\ F_{\mathrm{ext}} &= M\ddot{x} + B\dot{x} + (K + \alpha_K e)(x - x_{\mathrm{v}} - \alpha_x e) \end{aligned} \tag{8}$$

Using Euler's method as described in Equation (5), together with the formula for dynamic admittance from Equation (8), and solving for the displacement $(x_t - x_{\mathrm{v}})$ yields Equation (9),

$$\begin{aligned} x_t - x_{\mathrm{v}} = (x_{t-1} - (x_{\mathrm{v}} + \alpha_x e)) + \Delta t(\dot{x}_{t-1} \\ + \Delta t \left(\frac{1}{M}(F_{\mathrm{ext}} - B\dot{x} - (K + \alpha_K e)x_{t-1}) \right) \right). \end{aligned} \tag{9}$$

The update rules defined in Equations (6) and (7) seek to ensure safety, stability and robustness at the port of interaction. The gain α_x ensures kinematic consistency by formulating a virtual pose that tracks payload-relative motion. The gain α_K ensures force regulation as a function of inter-robot spacing by updating effective stiffness. While α_x was set to maintain a fixed virtual set point relative to the payload, α_K was set such that damping remains above the critical damping heuristic across the physical range of e.

Manipulator Heading The dynamic admittance controller adjusts the target position x along a single axis given a scalar force measurement F_{ext}, requiring the end-effector poses to remain collinear within the 2D special Euclidean group (SE(2)). To guarantee this, we calculate the heading adjustment θ_{M} and θ_{R} as diagrammed in Figure 2b via frame composition as described in Equations (10) and (11).

$$\mathbf{T}_{\mathbf{p}_{\mathrm{M_b}},\mathbf{p}_{\mathrm{R_b}}} = \mathbf{T}^{-1}_{\mathbf{p}_{\mathrm{M}},\mathbf{p}_{\mathrm{M_b}}}\ \mathbf{T}^{-1}_{\mathrm{W,M}}\ \mathbf{T}_{\mathrm{W,R}}\ \mathbf{T}_{\mathbf{p}_{\mathrm{R}},\mathbf{p}_{\mathrm{R_b}}} \tag{10}$$

$$\mathbf{T}_{\mathbf{p}_{\mathrm{R_b}},\mathbf{p}_{\mathrm{M_b}}} = \mathbf{T}^{-1}_{\mathbf{p}_{\mathrm{R}},\mathbf{p}_{\mathrm{R_b}}}\ \mathbf{T}^{-1}_{\mathrm{W,R}}\ \mathbf{T}_{\mathrm{W,M}}\ \mathbf{T}_{\mathbf{p}_{\mathrm{M}},\mathbf{p}_{\mathrm{M_b}}} \tag{11}$$

The desired manipulator rotation is $\mathrm{atan2}(y, x)$, where y and x are planar components of the translation vector $\mathbf{p} = [x\ y\ z]^\top$ in the homogeneous transformation. Specifically, we extract the last column of $\mathbf{T}_{\mathbf{p}_{\mathrm{M_b}},\mathbf{p}_{\mathrm{R_b}}}$ for Monica and $\mathbf{T}_{\mathbf{p}_{\mathrm{R_b}},\mathbf{p}_{\mathrm{M_b}}}$ for Ross.

Position Controlled Transportation A static position controller for the end-effector acts as a baseline for measuring the value of admittance control. In this control scheme, the end-effector maintains a fixed relative position located slightly inside the payload. For successful transportation, the JiANTs must maintain a fixed inter-robot distance.

2.2 Optimal Coordinated Planning

Successful mobile manipulation requires coordinated path planning for both agents. To do this, we parameterize the cooperative transport by considering the pose and dynamics of the payload $\mathbf{T}_{\mathrm{W,M}}(t) = [x(t), y(t), \phi]^\top \in \mathbb{R}^3$, following Slightam et al. (2025). The unit vectors defining the payload pose are

$$\hat{\mathbf{v}}(\phi) = \begin{bmatrix} \cos\phi \\ \sin\phi \end{bmatrix}, \hat{\mathbf{n}}(\phi) = \begin{bmatrix} -\sin\phi \\ \cos\phi \end{bmatrix}, r = \tfrac{L}{2} + a. \tag{12}$$

where r is the payload pose offset, $\hat{\mathbf{v}}$ is the unit tangent/forward direction of the payload (body x-axis) and $\hat{\mathbf{n}}$ is the unit normal/left direction (body y-axis) of the payload. A subset of $\mathbf{T}_{\mathrm{W,M}}$, to denote the x,y, positions is $\mathbf{c} = [x(t), y(t)]^T$. This can be used to define the base positions and velocities of the robots,

$$\mathbf{b}_1 = \mathbf{c} - r\hat{\mathbf{v}}, \qquad \mathbf{b}_2 = \mathbf{c} + r\hat{\mathbf{v}}, \tag{13}$$

$$\dot{\mathbf{b}}_1 = \dot{\mathbf{c}} - r\,\dot{\phi}\,\hat{\mathbf{n}}, \qquad \dot{\mathbf{b}}_2 = \dot{\mathbf{c}} + r\,\dot{\phi}\,\hat{\mathbf{n}}. \tag{14}$$

To determine the skid–steer platform headings (assuming no lateral slip) we define

$$\theta_i = \mathrm{atan2}((\dot{\mathbf{b}}_i)_y, (\dot{\mathbf{b}}_i)_x), \tag{15}$$

where θ_i are the base headings for Monica and Ross. With the geometry defined, the optimization problem can be setup where we aim to co–optimize 4 different components of the multi-agent motion. (1) minimum snap of the centerline: penalize $\|\mathbf{c}^{(4)}\|^2$. (2) minimum change of angular momentum: for a planar rigid body, $L_z = I_z\dot{\phi} \Rightarrow \dot{L}_z = I_z\ddot{\phi}$; penalize $\dot{L}_z^2 = I_z^2\ddot{\phi}^2$. (3) Soft yaw–tangent alignment: discourage large misalignment between box yaw ϕ and the tangent heading $\psi = \mathrm{atan2}(\dot{y}, \dot{x})$. Finally, (4) Tracking/boundary terms: keep the center-line close to a desired S-path between the start location and desired goal location and enforce boundary conditions.

The minimization function, J, is initially written for a strictly convex quadratic program (QP) as:

$$\begin{aligned} \min_{\mathbf{X},\mathbf{Y},\mathbf{\Phi}}\ J = w_{\mathrm{track}}\big(\|\mathbf{X} - \mathbf{X}^{\mathrm{ref}}\|_2^2 + \|\mathbf{Y} - \mathbf{Y}^{\mathrm{ref}}\|_2^2\big) \\ + w_{\mathrm{snap}}\big(\|D_4\mathbf{X}\|_2^2 + \|D_4\mathbf{Y}\|_2^2\big) \\ + w_{\dot{L}}\,\|D_2\mathbf{\Phi}\|_2^2 + w_{\ddot{L}}\,\|D_3\mathbf{\Phi}\|_2^2 \end{aligned} \tag{16}$$

D_i are co-state variables and the yaw–tangent coupling is left out initially. The Hessian is symmetric positive definite (SPD), so Equation (16) solves in $\mathcal{O}(N)$ with a band solver. The term, w_{snap}, limits center-line jerkiness; $w_{\dot{L}}$ penalizes torque effort (since $\tau_z = \dot{L}_z = I_z\ddot{\phi}$); $w_{\ddot{L}}$ limits torque *rate*.

We reintroduce the constraints for the yaw to follow the tangent heading $\psi = \mathrm{atan2}(\dot{y}, \dot{x})$, but ψ is nonconvex in $(\mathbf{X}, \mathbf{Y})$. We add a quadratic *alignment* term and linearize it about the previous iterate.

To achieve coupling in sequence we require the linearization of the heading map, by letting $\dot{x}_k = (D_1\mathbf{X})_k,\ \dot{y}_k =$

$(D_1\mathbf{Y})_k$, $s_k^2 = \dot{x}_k^2 + \dot{y}_k^2$, $\psi_k = \operatorname{atan2}(\dot{y}_k, \dot{x}_k)$. Its first variation is

$$\delta\psi_k = \frac{\partial\psi_k}{\partial\dot{x}_k}\delta\dot{x}_k + \frac{\partial\psi_k}{\partial\dot{y}_k}\delta\dot{y}_k = \Big(-\frac{\dot{y}_k}{s_k^2}\Big)\delta\dot{x}_k + \Big(\frac{\dot{x}_k}{s_k^2}\Big)\delta\dot{y}_k.$$

Since $\delta\dot{x} = D_1\,\delta\mathbf{X}$, $\delta\dot{y} = D_1\,\delta\mathbf{Y}$, the linearized alignment residual at iterate j is

$$\begin{aligned} r^{(j)} = {} & \underbrace{(\mathbf{\Phi} - \mathbf{\Phi}^{(j)})}_{\text{yaw increment}} + \underbrace{(\mathbf{\Phi}^{(j)} - \mathbf{\Psi}^{(j)})}_{\text{constant}} \\ & \underbrace{- P_x^{(j)} D_1(\mathbf{X} - \mathbf{X}^{(j)}) + P_y^{(j)} D_1(\mathbf{Y} - \mathbf{Y}^{(j)})}_{\text{tangent increment}}, \end{aligned} \tag{17}$$

with diagonal gains $P_x^{(j)} = \operatorname{diag}\big(-\dot{y}_k^{(j)}/s_k^{(j)2}\big)$, $P_y^{(j)} = \operatorname{diag}\big(\dot{x}_k^{(j)}/s_k^{(j)2}\big)$, and $\mathbf{\Psi}^{(j)} = [\psi_k^{(j)}]$. We add $w_{\text{align}}\|r^{(j)}\|_2^2$ to the cost. This produces only quadratic (and banded) cross terms between $\mathbf{X}, \mathbf{Y}, \mathbf{\Phi}$.

Equation (18) extends the cost function defined in Equation (16) by adding an alignment term. At each iteration j we solve the convex QP,

$$\min_{\mathbf{X},\mathbf{Y},\mathbf{\Phi}} J(\mathbf{X}, \mathbf{Y}, \mathbf{\Phi}) + w_{\text{align}}\|r^{(j)}(\mathbf{X}, \mathbf{Y}, \mathbf{\Phi})\|_2^2, \tag{18}$$

subject to boundary equalities (position, and zero end velocities or yaw rates) and payload bounds. Following this, $(\mathbf{X}^{(j+1)}, \mathbf{Y}^{(j+1)}, \mathbf{\Phi}^{(j+1)}) \leftarrow (\mathbf{X}, \mathbf{Y}, \mathbf{\Phi})$ is set and repeated until convergence occurs (small change of J or of the variables).

Once $(\mathbf{X}, \mathbf{Y}, \mathbf{\Phi})$ are found, we iteratively determine the terms in Equations (12) to (15), described via Algorithm 1 using a sequential convex quadratic program (SCQP).

Closed-Loop Control Architecture Desired positions, $B_{1,k}, B_{2,k}$, and headings, $\theta_{1,k}, \theta_{2,k}$, at step k from Algorithm 1 are recovered via Equations (13) and (15), while measured positions $\hat{B}_{1,k}$, $\hat{B}_{2,k}$, $\hat{\theta}_{1,k}$, and $\hat{\theta}_{2,k}$ come from the Vicon system. Typical of skid-steer mobile platforms, we implement a PID controller that maps longitudinal error to linear command velocities, and a cascaded PD-PID controller that maps lateral and heading error to angular command velocities.

Algorithm 1 SCQP for snap+$\dot{L}$ co–optimization

Build S–path samples $\mathbf{X}^{\text{ref}}, \mathbf{Y}^{\text{ref}}$ & initial $\mathbf{\Phi}^{(0)}$
Initialize $\mathbf{X}^{(0)} = \mathbf{X}^{\text{ref}}$, $\mathbf{Y}^{(0)} = \mathbf{Y}^{\text{ref}}$.
for $j = 0, 1, 2, \ldots$ **do**
    Compute $\dot{x}^{(j)} = D_1\mathbf{X}^{(j)}$, $\dot{y}^{(j)} = D_1\mathbf{Y}^{(j)}$, $s^{(j)} = \sqrt{\dot{x}^{(j)2} + \dot{y}^{(j)2}}$, $\mathbf{\Psi}^{(j)} = \operatorname{atan2}(\dot{y}^{(j)}, \dot{x}^{(j)})$.
    Form $P_x^{(j)} = \operatorname{diag}(-\dot{y}^{(j)}/s^{(j)2})$, $P_y^{(j)} = \operatorname{diag}(\dot{x}^{(j)}/s^{(j)2})$.
    Solve the convex QP 18 with boundary equalities (banded SPD).
    Update $\mathbf{X}^{(j+1)}, \mathbf{Y}^{(j+1)}, \mathbf{\Phi}^{(j+1)} \leftarrow \mathbf{X}, \mathbf{Y}, \mathbf{\Phi}$.
    if $J^{(j)} - J^{(j+1)} < \varepsilon$ and $\|(\mathbf{X}^{(j+1)}, \mathbf{Y}^{(j+1)}, \mathbf{\Phi}^{(j+1)}) - (\mathbf{X}^{(j)}, \mathbf{Y}^{(j)}, \mathbf{\Phi}^{(j)})\| < \varepsilon$ **then break**
    end if
end for
Recover $\mathbf{b}_{1,2}, \dot{\mathbf{b}}_{1,2}, \theta_{1,2}$ via Equations (13) to (15).

Positions are decomposed $B_{i,k} = [x_{i,k}, y_{i,k}]^\top$ and then transformed into the mobile base frame via $\mathbf{T}_{\text{W,M}}$ and $\mathbf{T}_{\text{W,R}}$. Longitudinal error in the mobile base frame $e_{i,k}^x = x_{i,k} - \hat{x}_{i,k}$ is passed into a PID controller which produces $\dot{x}_{\text{cmd}}$, a linear command velocity. Lateral and heading errors are combined into a single angular command velocity about the z-axis. Lateral error $e_{i,k}^y = y_{i,k} - \hat{y}_{i,k}$, is passed through a PD controller which produces a $\theta_{d,k}$ correction, then error $e_{i,k}^\theta = \theta_{d,k} + \theta_{i,k} - \hat{\theta}_{i,k}$ is passed through a PID controller which produces $\dot{\theta}_{\text{cmd}}$, an angular command velocity about the z-axis.

2.3 Experimental Methods

Hardware Implementation Ross and Monica are skid-steer JiANT robots designed to be assembled by students and are built from low-cost commodity components and 3D printed parts. A PincherX-100 4-DOF robotic arm by Trossen Robotics and a low-cost, consumer grade 38×38 mm force-sensing resistor (FSR) by Interlink Electronics are equipped. As can be seen in Figure 1, the pincher was replaced with a 3D printed flat-plate end-effector equipped with an FSR. Each robot uses four Pololu brushed DC motors controlled by a Teensy 4.0, which was programmed using Arduino and micro-ROS to move the wheels. An Intel NUC mounted on the JiANT runs robot operating system version 2 (ROS2) nodes. We replaced the soft rubber tires with hard 3D printed wheels for better drive actuation and encoder-based odometry. The JiANT base is 24 cm long and 33 cm wide.

The payload is a small untreated cardboard box of mass 87 g (Figure 1). Note that this is greater than the individual payload of each manipulator. Because the JiANT mobile robots do not have on board vision, a laboratory Vicon tracking system was borrowed. This centralized perception source supplied pose data to each robot to all robots in the system which allows for the error in the inter-robot distance e, to be available to the distributed control algorithms.

Experimental Setup We test three different control strategies: admittance control (Section 2.1.1), dynamic parameterization (Section 2.1.2), and position control (Section 2.1.4). All three strategies share the planner and tracking method (Section 2.2), isolating the effect of the manipulator controller. Each strategy was evaluated on a set of 20 trials, in which the robots were commanded to transport a pre-loaded payload along either a right or left S-shaped path generated by the planner to introduce a variety in trajectory direction. The point at which the payload drops is noted by video and the forces applied to the end effectors. We classify successful trials as "perfect" or "faulty" (which indicates that the payload shifted or twisted visibly during transport, but did not fall). Although technically reaching the goal, faulty indicated an insecure hold on the payload.

Results are presented as distance traveled and success rate (Figure 4). Trials affected by hardware and software issues (e.g. failed servos and ROS2 initialization problems) unrelated to the strategy being tested were excluded. These failures constituted less than 10% of total trials. Furthermore, the Vicon system was used to measure the trajectory of the robots and the payload over time.

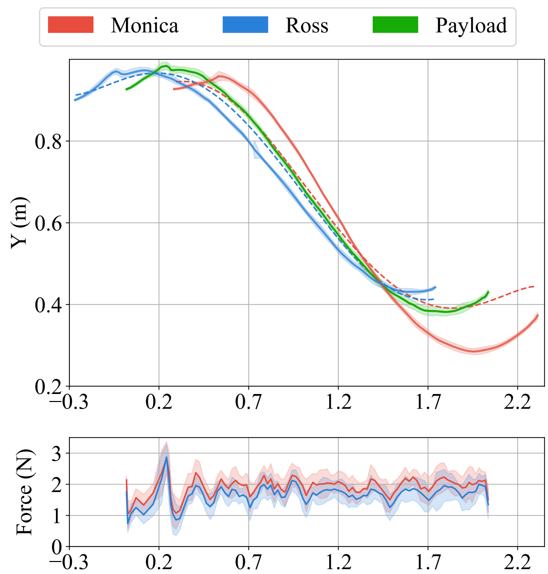

Fig. 3. Desired position (dashed line), mean position (solid line), and standard deviation (shaded area) for motion along an s-curve. The force plots, aligned with trajectory along the x-axis, show that mean force (solid line) and standard deviation (shaded area) are steadily maintained throughout transport.

3. RESULTS

Figure 3 shows the trajectory and interaction forces recorded under the dynamic admittance controller. Although the applied forces fluctuate, they remain bounded, never exceeding the mechanical limits of the manipulators, and apply moderate, well-regulated contact forces that keep the payload secure. This suggests that the dynamic admittance controller is actively modulating compliance to accommodate unmodeled dynamics and mobile base errors. The effectiveness of DYNAMO is evident in Figure 4, which shows the distance traveled before the payload was dropped using each strategy. The dynamic admittance controller consistently reached the full 2.2 m extent of the trajectory, limited only by the geometry of the Vicon workspace, while the position and static admittance controllers failed to come close.

As shown in Figure 4, the dynamic admittance controller achieved a 100% success rate, completing all 20 trials without dropping the payload. In contrast, the static admittance controller completed only one perfectly successful trial, and the position controller failed in all attempts. The position controller had a mean transport distance of 0.13 m (95% CI [0.11 m, 0.16 m]), the static admittance controller 0.96 m (95% CI [0.52 m, 1.4 m]), and the dynamic admittance parameterization controller 2.2 m (limited by the arena size). Dynamic admittance achieved a significantly greater transport distance than both position control (mean difference 2.1 m, Welch's t-test, $p \ll 0.001$) and static admittance (mean difference 1.2 m, $p < 0.001$). Static admittance also exceeded position control (mean difference 0.82 m, $p < 0.001$).

Experimental data is available online.[1] as is the code used to implement the position, admittance, and DYNAMO controllers.

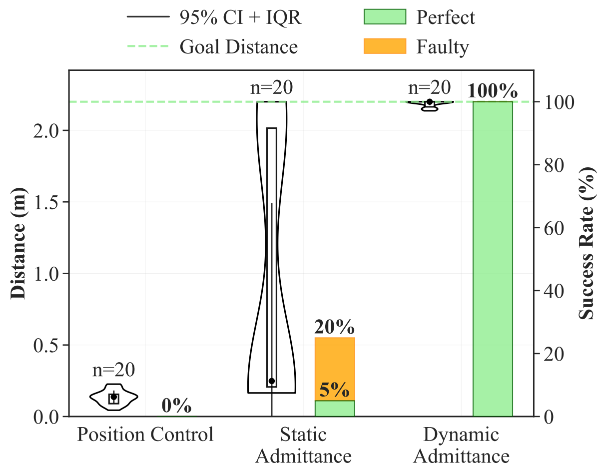

Fig. 4. Combined chart showing both distance traveled and success rate. Boxes show inter-quartile range; vertical black lines indicate 95 % confidence intervals for the median. Closed circles denote medians: 0.13 m (position), 0.21 m (admittance), and 2.2 m (dynamic admittance). Green bars show percentage of successful trials; orange bars indicate faulty trials.

4. DISCUSSION

The success of DYNAMO arises from its ability to modulate compliance in real-time based on sensed interaction forces, which enables it to maintain sufficient end-effector contact with the payload. The force traces in Figure 3 show that the controller maintains applied forces in a bounded, effective range, avoiding both excessive pressure that could destabilize the system and insufficient contact that would drop the payload. The position controller, which provided no compensation via the arms to correct for accumulated or sudden base displacement, failed to transport the payload entirely. The static admittance controller offered limited improvement, completing only one successful trial and 5 faulty trials. Its inability to handle growing positional errors stems from its fixed admittance parameters, which cannot adapt to changing conditions or external disturbances. Dynamic admittance parameterization overcame these shortcomings by using feedback to adjust interaction behavior on the fly. It allowed the system to respond to conditions that are difficult to model, avoided the need for exact identification of the payload's inertial or frictional properties, and is generalizable to new hardware, tasks, or robot configurations, making it especially suitable for distributed and heterogeneous multi-robot systems under a centralized or global perception signal.

Experiments captured only a subset of the multi-robot cooperative transport problem. Trials were conducted in a constrained Vicon workspace on a limited set of S-curve trajectories. Future work should explore a broader range of trajectories, including endurance tests on circular or

[1] https://anonymous.4open.science/r/MARIAM-8746/README.md

figure-eight paths, perform sensitivity tests across diverse payload materials, weights, and sizes, and transition from centralized perception to onboard localization to support deployment in unstructured real-world environments.

More broadly, these results highlight the potential of adaptive compliance in distributed cooperative manipulation. By tuning admittance in response to sensed error, the system remains robust to disturbances without requiring explicit coordination or communication of internal states, making the approach both scalable and tolerant to partial failures. Successful mobile manipulation also requires coordinated path planning that accounts for coupled motion. The optimal navigation planner and the dynamic admittance parameterization controller provide a practical solution to non-prehensile multi-robot manipulation tasks in which grasping the payload is not possible.

ACKNOWLEDGEMENTS

This work was supported by Sandia subcontract 2417427, i.e., Multi-Agent Robust Intelligent Autonomous Manipulation (MARIAM) under LDRD 229360: Science of Intelligent Autonomous Manipulation (SIAM). The authors would like to thank Fernando Moreu and his PhD student Mahsa Sanei of the Smart Management of Infrastructure Laboratory (SMILab) for providing access to their Vicon camera system. The Vicon work was supported by the Office of Naval Research, Structural Reliability ONR 331 under Grant No. 13620990 (Award No. N00014-22-1-2638) and Grant No. 13106652 (Award No. N00014-21-1-2929). We are grateful to Carter Frost for helpful discussions and early contributions to this work.

REFERENCES

Amirkhani, A. and Barshooi, A.H. (2022). Consensus in multi-agent systems: a review. *Artificial Intelligence Review*, 55(5), 3897–3935.

An, X., Wu, C., Lin, Y., Lin, M., Yoshinaga, T., and Ji, Y. (2023). Multi-robot systems and cooperative object transport: Communications, platforms, and challenges. *IEEE Open Journal of the Computer Society*, 4, 23–36.

Barawkar, S., Radmanesh, M., Kumar, M., and Cohen, K. (2017). Admittance Based Force Control for Collaborative Transportation of a Common Payload Using Two UAVs. In *Volume 3: Vibration in Mechanical Systems*, 39. American Society of Mechanical Engineers, Tysons, Virginia, USA.

Carey, N.E. and Werfel, J. (2021). Collective transport of unconstrained objects via implicit coordination and adaptive compliance. In *2021 IEEE International Conference on Robotics and Automation (ICRA)*, 12603–12609. IEEE.

Chen, J. and Kai, S. (2018). Cooperative transportation control of multiple mobile manipulators through distributed optimization. *Science China Information Sciences*, 61(12).

Duan, J., Gan, Y., Chen, M., and Dai, X. (2018). Adaptive variable impedance control for dynamic contact force tracking in uncertain environment. *Robot. Auton. Syst.*, 102(C), 54–65.

Gholampour, H., Slightam, J.E., and Beaver, L. (2025). Mass-adaptive admittance control for robotic manipulators. In *2025 Modeling, Estimation and Control Conference (MECC)*. IFAC.

Hichri, B., Fauroux, J.C., Adouane, L., Doroftei, I., and Mezouar, Y. (2019). Design of cooperative mobile robots for co-manipulation and transportation tasks. *Robotics and Computer-Integrated Manufacturing*, 57, 412–421.

Hogan, N. and Buerger, S. (2004). Impedance and Interaction Control. In T. Kurfess (ed.), *Robotics and Automation Handbook*. CRC Press.

Jinyan Shao, Guangming Xie, Junzhi Yu, and Long Wang (2005). Leader-Following Formation Control of Multiple Mobile Robots. In *Proceedings of the 2005 IEEE International Symposium on, Mediterrean Conference on Control and Automation Intelligent Control, 2005.*, 808–813. IEEE.

Li, Y., Yang, C., Yan, W., Cui, R., and Annamalai, A. (2019). Admittance-based adaptive cooperative control for multiple manipulators with output constraints. *IEEE transactions on neural networks and learning systems*, 30(12), 3621–3632.

Liu, Z. and Miah, M.S. (2024). Cooperative Object Transportation Using Autonomous Networked Cobots: A Distributed Approach. In *2024 IEEE International Symposium on Robotic and Sensors Environments (ROSE)*, 1–7. IEEE, Chemnitz, Germany.

McArthur, D.R., Slightam, J.E., Spencer, S.J., and Buerger, S.P. (2024). Coordinated admittance-impedance control with force excitation for compliant, underactuated aerial manipulation. *IFAC-PapersOnLine*, 58(28), 558–563. The 4th Modeling, Estimation, and Control Conference – 2024.

Newman, W.S. (1992). Stability and performance limits of interaction controllers. *Journal of Dynamic Systems, Measurement, and Control*, 114(4), 563–570.

Qin, D., Wu, J., Liu, A., Zhang, W.A., and Yu, L. (2022). Cooperation and coordination transportation for nonholonomic mobile manipulators: A distributed model predictive control approach. *IEEE Transactions on Systems, Man, and Cybernetics: Systems*, 53(2), 848–860.

Slightam, J.E. and Griego, A.D. (2023). Deep neural network design for improving stability and transient behavior in impedance control applications. In *2023 ASME/IEEE International Conference on Advanced Intelligent Mechatronics (AIM)*. ASME/IEEE.

Slightam, J.E., McArthur, D.R., Spencer, S.J., and Buerger, S.P. (2021). Passivity analysis of quadrotor aircraft for physical interactions. In *2021 Aerial Robotic Systems Physically Interacting with the Environment (AIRPHARO)*. IEEE.

Slightam, J.E., Steyer, A.J., Beaver, L.E., and Young, C.C. (2025). An approach to realize generalized optimal motion primitives using physics informed neural networks. *Letters in Dynamic Systems and Control*, 5(2).

Tuci, E., Alkilabi, M.H., and Akanyeti, O. (2018). Cooperative object transport in multi-robot systems: A review of the state-of-the-art. *Frontiers in Robotics and AI*, 5, 59.

Yufka, A. and Ozkan, M. (2015). Formation-based control scheme for cooperative transportation by multiple mobile robots. *International Journal of Advanced Robotic Systems*, 12(9), 120.